


Vanadium 3d charge and orbital states in V₂OPO₄ probed by x-ray absorption spectroscopyKota Murota,¹ Elise Pachoud,² J. Paul Attfield,² Robert Glaum³,³ Ronny Sutarto,⁴ Kou Takubo⁵,⁵
Daniel I. Khomskii,⁶ and Takashi Mizokawa¹¹Department of Applied Physics, Waseda University, Shinjuku, Tokyo 169-8555, Japan²Centre for Science at Extreme Conditions and School of Chemistry, University of Edinburgh, Edinburgh EH9 3FD, United Kingdom³Institut für Anorganische Chemie, Universität Bonn, D-53012 Bonn, Germany⁴Canadian Light Source, Saskatoon, Saskatchewan, Canada S7N 0X4⁵Department of Chemistry, Tokyo Institute of Technology, Meguro, Tokyo 152-8551, Japan⁶II Physikalisches Institut, Universität zu Köln, D-50937 Köln, Germany (Received 19 January 2020; revised manuscript received 9 April 2020; accepted 19 May 2020; published 1 June 2020)

V 3d charge and orbital states in V₂OPO₄ have been investigated by means of x-ray absorption spectroscopy (XAS). The electronic structure of V₂OPO₄ is very unique in that the charge transfer between V²⁺ and V³⁺ in face-sharing VO₆ chains provides negative thermal expansion as reported by E. Pachoud *et al.* [*J. Am. Chem. Soc.* **140**, 636 (2018)]. The near-edge region of O 1s XAS exhibits the three features which can be assigned to transitions to O 2p mixed into the unoccupied V 3d t_{2g} and e_g orbitals of V²⁺ and V³⁺. The V 2p XAS line shape can be reproduced by multiplet calculations for a mixed-valence state with V²⁺ and V³⁺. The polarization dependence of the O 1s and V 2p XAS spectra indicates V 3d orbital order in which xy and yz (or zx) orbitals are occupied at the V³⁺ site in the face-sharing chains. The occupied xy orbital is essential for the antiferromagnetic coupling between the V²⁺ and V³⁺ sites along the chains, while the occupied yz (or zx) orbital provides the antiferromagnetic coupling between the V²⁺ and V³⁺ sites between the chains.

DOI: [10.1103/PhysRevB.101.245106](https://doi.org/10.1103/PhysRevB.101.245106)

I. INTRODUCTION

Transition-metal compounds have been attracting great interest due to their rich lattice and electronic properties, which are derived from the transition-metal *d* and ligand *p* orbitals [1,2]. The interplay between the lattice and electronic properties provides an exotic phenomenon known as negative thermal expansion (NTE) through rigid-bond formation, the magnetoelastic effect, and the charge transfer effect [3–6]. The charge transfer mechanism for NTE is characterized by a dramatic valence change in transition metals. For example, BiNiO₃ exhibits a valence transition from insulating Bi³⁺Bi_{0.5}Ni_{0.5}O₃ to metallic Bi³⁺Ni³⁺O₃ under high pressure [7–9]. La substitution for Bi suppresses the insulating state, and the moderate NTE is realized at ambient pressure in Bi_{1-x}La_xNiO₃ [10–12].

Very recently, Pachoud *et al.* reported NTE in V₂OPO₄ which is driven by charge transfer between V²⁺ and V³⁺ sites [13]. V₂OPO₄ consists of face- and corner-sharing VO₆ octahedra, as shown in Fig. 1. Below 605 K, the V²⁺/V³⁺ charge ordering is accompanied by monoclinic lattice distortion [13]. The face-sharing V²⁺ and V³⁺ sites form chains along the [110] or [1 $\bar{1}$ 0] direction of the monoclinic lattice, as indicated by the dashed lines in Fig. 1. The corner-sharing V³⁺ sites are connected approximately along the [001] direction. The VO₆ octahedra in the [1 $\bar{1}$ 0] chains are tilted relative to those in the [110] chains. In Fig. 1, the *x*, *y*, and *z* axes are along the V-O bonds of the V³⁺ site in the [110] chain, while the *x'*, *y'*, and *z'* axes are along the V-O bonds of the V³⁺ site in the [1 $\bar{1}$ 0] chain. The V²⁺/V³⁺ spins are ferrimagnetically ordered

below 165 K. The V²⁺ and V³⁺ spins are antiferromagnetically coupled along the face-sharing bond, and the V³⁺ spins are ferromagnetically coupled along the corner-sharing bond [13]. Above 165 K, the magnetic susceptibility shows a paramagnetic moment of 1.61μ_B per V₂OPO₄ unit, which is greatly reduced from the ideal value for V²⁺ and V³⁺ spins [13]. Above 605 K, the charge ordering disappears, and all the V sites become V^{2.5+} in tetragonal lattice structure. Since the tetragonal phase with V^{2.5+} has a smaller volume than the monoclinic phase with V²⁺ and V³⁺, NTE is realized around 605 K [13]. The NTE in V₂OPO₄ is seen at relatively high temperature compared to Bi_{1-x}La_xNiO₃. As for the mechanism of the charge transfer transition, the availability of single crystals enables us to study the role of V 3d orbital ordering. Soft x-ray absorption spectroscopy is a powerful technique to study valence and orbital states of V. In the present work, we study V 3d orbital states by means of polarization-dependent x-ray absorption measurement and cluster model analysis.

II. METHODS

X-ray absorption spectroscopy (XAS) measurement was performed at the Resonant Elastic and Inelastic X-ray Scattering (REIXS) beamline of the Canadian Light Source [15]. The incident soft x ray is linearly polarized. XAS spectra were taken in the total electron yield (TEY) mode and total fluorescence yield (TFY) mode. The single crystal was mounted in such a way that polarization vectors of the incident soft x ray are along the [001] axis for the horizontal polarization and along the [221] axis for the vertical polarization.

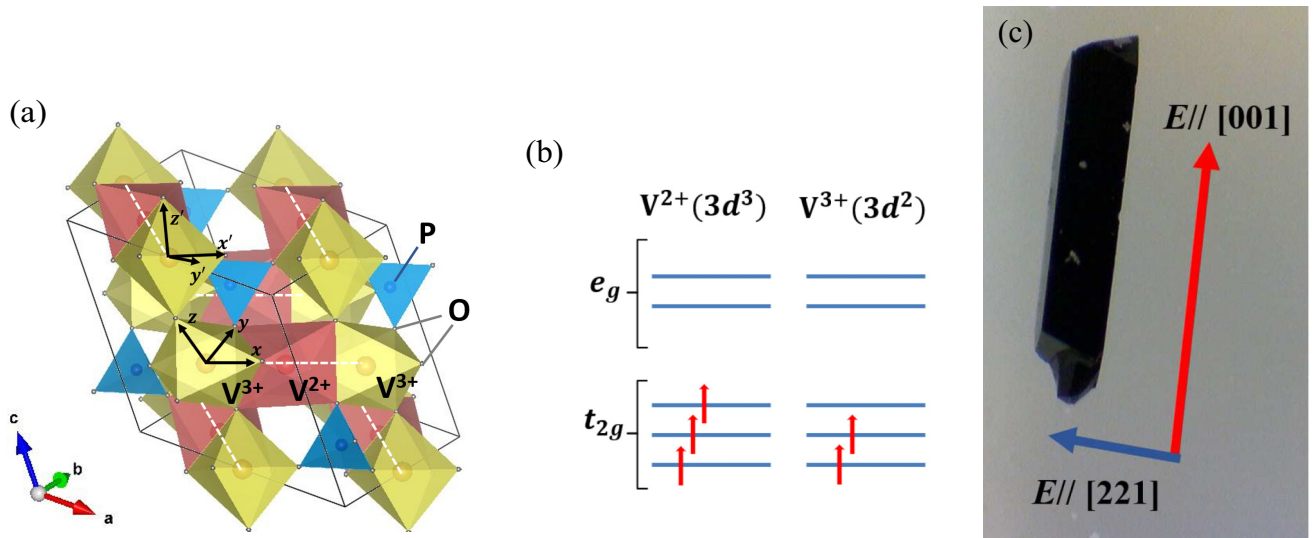


FIG. 1. (a) Crystal structure of V₂OPO₄ created by VESTA [14]. The dashed lines indicate the face-sharing VO₆ chains along the [110] or [1̄10] directions. The x , y , and z axes (x' , y' , and z' axes) are along the V-O bonds of the V³⁺ site in the [110] chain ([1̄10] chain). (b) Electronic configurations for V²⁺ and V³⁺. (c) Photograph of the V₂OPO₄ crystal and the directions of the polarization vector.

The XAS spectra can be analyzed by the VO₆ cluster model calculations. In the present analysis, the O 2*p* to V 3*d* charge transfer process is neglected since the charge transfer energies for V³⁺ and V²⁺ oxides are typically around 6 and 8 eV, respectively [16,17]. In the present cluster model, the ligand field splitting between e_g and t_{2g} levels ($10Dq$) is fixed to 1.6 eV. The Coulomb interaction between the V 3*d* electrons is given by the Slater integrals $F^2(3d, 3d)$ and $F^4(3d, 3d)$, which can be translated into Racah parameters B and C . In the present analysis, B and C are set to 0.117 and 0.438 eV [16,17]. The Coulomb interaction between the V 2*p* core hole and the V 3*d* electron is expressed by the Slater integrals $F^2(2p, 3d)$, $G^1(2p, 3d)$, and $G^3(2p, 3d)$, which are fixed to 4.85, 3.51, and 2.00 eV, respectively (about 80% of the atomic Hartree-Fock values) [18]. When the effect of the charge transfer process is examined, the transfer integrals are parameterized by Slater-Koster parameters ($pd\sigma$) and ($pd\pi$) with $(pd\pi)/(pd\sigma) = -0.45$. In the final states with a core hole, the magnitude of transfer integrals is multiplied by 0.8, considering the contraction of 3*d* wave functions due to the core hole potential [19,20]. For the V³⁺ case, the charge transfer energy Δ (multiplet averaged), V 3*d*-3*d* Coulomb interaction U (multiplet averaged), and V 2*p*-3*d* Coulomb interaction Q (multiplet averaged) are fixed to 6.0, 5.0, and 6.0 eV, respectively. Also $10Dq$ due to nonorthogonality is considered [20].

Local-density approximation (LDA)+ U calculations were performed using QUANTUM ESPRESSO 5.30 [21,22]. We employed pseudopotentials of V.pz-spnl-kjpaw_psl.1.0.0.UPF, O.pz-n-kjpaw_psl.0.1.UPF, and P.pz-n-kjpaw_psl.0.1.UPF. U and J are fixed to 5.0 and 0.5 eV, respectively. The cutoff energy was set to 30 Ry.

III. RESULTS AND DISCUSSION

Figure 2 shows O 1*s* XAS spectra taken with the polarization vector along the [001] direction (dashed curves) and

with that along the [221] direction (solid curves) at various temperatures well below the structural transition temperature at 605 K. The spectra are normalized with respect to intensities at 529 and 558 eV. The near-edge region from 530 to 535 eV corresponds to the excitations from O 1*s* to O 2*p* mixed into unoccupied V 3*d* levels. In the case of LiVO₂ with octahedrally coordinated V³⁺ (t_{2g}^3), the transition to t_{2g}^3 and those to $t_{2g}^2 e_{g\uparrow}$, $t_{2g}^2 t_{2g\downarrow}$, and $t_{2g}^2 e_{g\downarrow}$ are located around 530 and 532 eV, respectively [23]. In the O 1*s* XAS spectra of V₂OPO₄, the broad and weak peak at 531 eV corresponds to the transition to t_{2g}^3 at V³⁺. The peaks at 533 and 534 eV can be assigned to the transitions to $t_{2g}^2 e_{g\uparrow}$, $t_{2g}^2 t_{2g\downarrow}$, and $t_{2g}^2 e_{g\downarrow}$ at V³⁺ and the transitions from t_{2g}^3 to $t_{2g}^3 e_{g\uparrow}$, $t_{2g}^3 t_{2g\downarrow}$, and $t_{2g}^3 e_{g\downarrow}$ at V²⁺.

The peak at 531 eV is enhanced by the polarization vector along the [001] axis, as shown in the difference spectra in Fig. 2(c). This polarization dependence of the 531 eV peak is more clearly seen in the bulk-sensitive TFY spectra in Fig. 2(d) and indicates that the unoccupied t_{2g} orbital at V³⁺ is mainly mixed with O 2*p_z* orbitals along the [001] axis. Therefore, the unoccupied $t_{2g\uparrow}$ orbital in the V³⁺ (t_{2g}^3) site has either yz or zx symmetry in which the z axis is slightly tilted from the [001] direction and the x axis is approximately along the [201] direction for the V³⁺O₆ octahedra in the [110] chains, as indicated in Fig. 1(a). As for the other half of V³⁺O₆ octahedra in the [1̄10] chains, the z' axis is tilted in the other direction from the [001] direction, as shown in Fig. 1(a). Although the polarization dependence of the O 1*s* XAS spectra should be the average of the two kinds of V³⁺O₆ octahedra, it is still roughly consistent with the unoccupied zx or yz ($z'x'$ or $y'z'$) orbital. Indeed, the VO₆ octahedron for the V³⁺ site is compressed along the z or z' direction [13], and therefore, the xy ($x'y'$) orbital is stabilized by the ligand field. (The V-O bond length along the z (z') direction is ~ 1.98 Å, and those along the x (x') and y (y') directions are ~ 2.09 and 2.05 Å [13].) In addition to the polarization

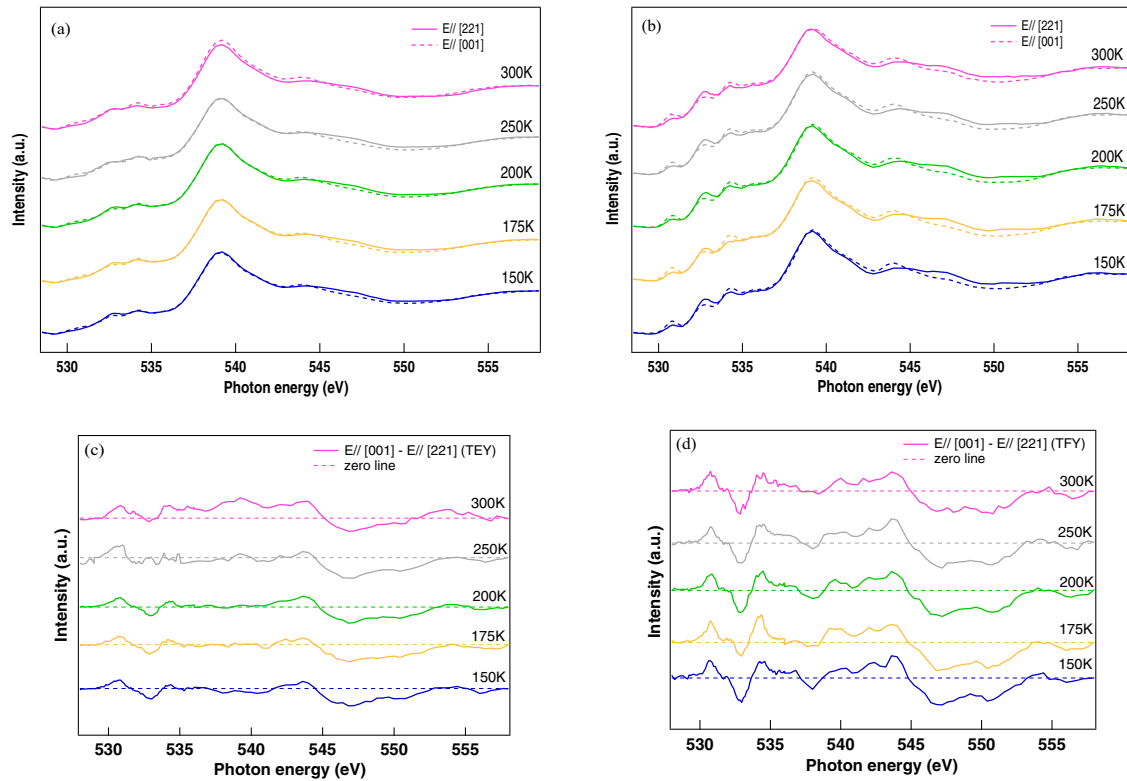


FIG. 2. (a) Temperature and polarization dependence of O 1s XAS with the TEY mode. (b) Temperature and polarization dependence of O 1s XAS with the TFY mode. (c) Temperature dependence of linear dichroism in O 1s XAS with the TEY mode. (d) Temperature dependence of linear dichroism in O 1s XAS with the TFY mode.

dependence of the 531-eV peak due to the t_{2g} orbital ordering, the peaks at 533 and 534 eV also depend on the polarization, probably due to the anisotropic hybridization between V 3d and O 2p orbitals by the distortion of the VO₆ octahedra. As shown in Figs. 2(c) and 2(d), the temperature dependence of the O 1s spectra is rather small, indicating the V 3d electronic state is not affected by the magnetic transition at 165 K.

Figure 3 shows V 2p XAS spectra taken with the polarization vector along the [001] direction (dashed curves) and with that along the [221] direction (solid curves) at various temperatures well below the structural transition temperature of

605 K. The spectra are normalized with respect to intensities at 510 and 529 eV. The multiplet structure in the near-edge region around 514 eV is derived from the V³⁺ component [18]. The overall multiplet structure is rather similar to that of LiVO₂ [23] in the surface-sensitive TEY spectra. However, the intensity around 523 eV is enhanced, suggesting the existence of V²⁺. In order to demonstrate the mixed valence of V²⁺ and V³⁺, calculated V 2p spectra for V²⁺ and V³⁺ are mixed to reproduce the experimental results, as shown in Fig. 4. The surface-sensitive TEY spectra can be explained with an ~30% contribution of V²⁺ relative to V³⁺, suggesting

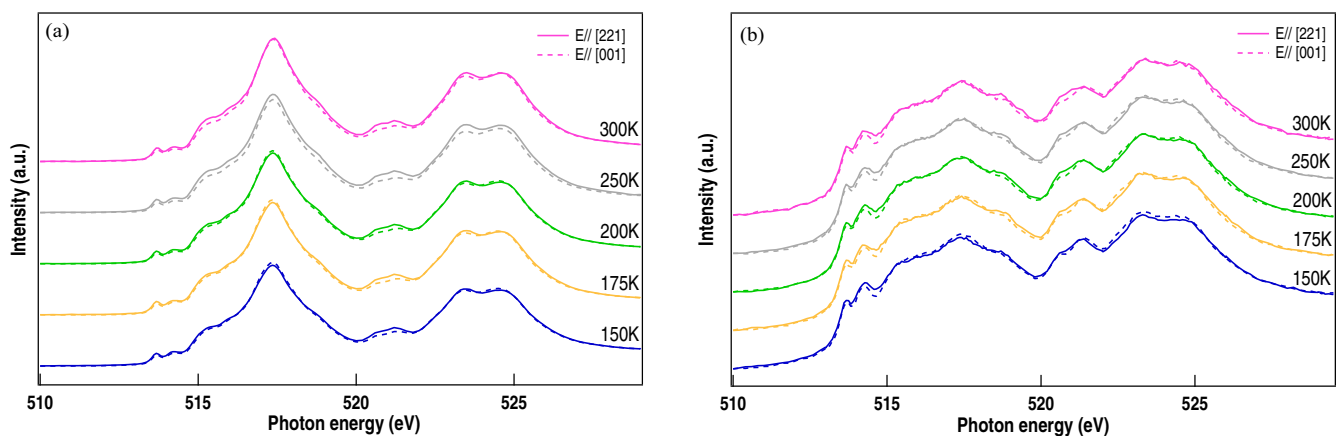


FIG. 3. (a) Temperature and polarization dependence of V 2p XAS with the TEY mode. (b) Temperature and polarization dependence of V 2p XAS with the TFY mode.

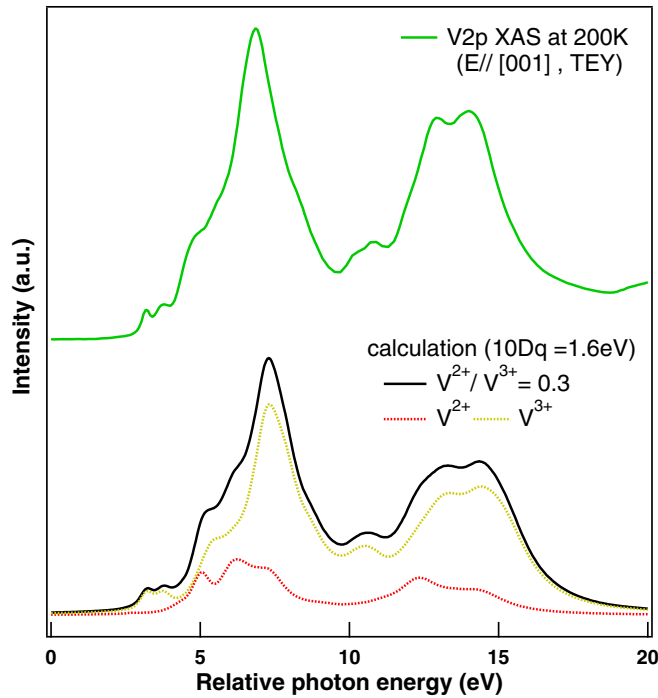


FIG. 4. Cluster model calculation of V $2p$ XAS for a mixed-valence state of $V^{2+} : V^{3+} = 3 : 10$. The calculated spectrum is compared with the experimental result taken at 200 K with the TEY mode.

a mixed-valence state. However, the amount of V^{2+} is much smaller than that expected from the charge order in the bulk. Most likely, the V^{3+} component is enhanced near the surface compared to the bulk value since the surface was exposed to the air. As for the bulk-sensitive TFY spectra, it is difficult to analyze the line shape quantitatively since it is affected by the self-absorption effect and the saturation effect. However, as shown in Fig. 3, the intensities around 516 and 523 eV (corresponding to 6 and 13 eV in the calculation shown in Fig. 4) are enhanced in the TFY spectra compared to the TEY spectra, indicating that the V^{2+} component increases in the bulk-sensitive TFY spectra compared to that in the surface-sensitive TEY spectra.

In the near-edge regions around 514 eV for $2p_{3/2}$ and around 521 eV for $2p_{1/2}$, the V $2p$ spectral weight is slightly enhanced with the polarization vector along the $[221]$ direction. Since the near-edge regions correspond to the transitions from V $2p$ to unoccupied V $3d t_{2g}$ at the V^{3+} site, the polarization dependence in the near-edge regions includes information on the V $3d$ orbital order. In V_2O_3 , Park *et al.* revealed that the intensity of the near-edge regions is enhanced when the a_{1g} orbital along the c axis is unoccupied and the polarization vector is parallel to the c axis [24]. In the case of Ti_2O_3 , the intensity of the near-edge regions is enhanced if the a_{1g} orbital along the c axis is occupied and the polarization vector is perpendicular to the c axis [25]. Here, the a_{1g} orbital is given by a linear combination of the xy , yz , and zx orbitals as $(xy + yz + zx)/\sqrt{3}$. Since the a_{1g} orbital does not change its sign under the rotation about the principal axis or the (111) axis, the relationship between the polarization and the intensity is rather simple.

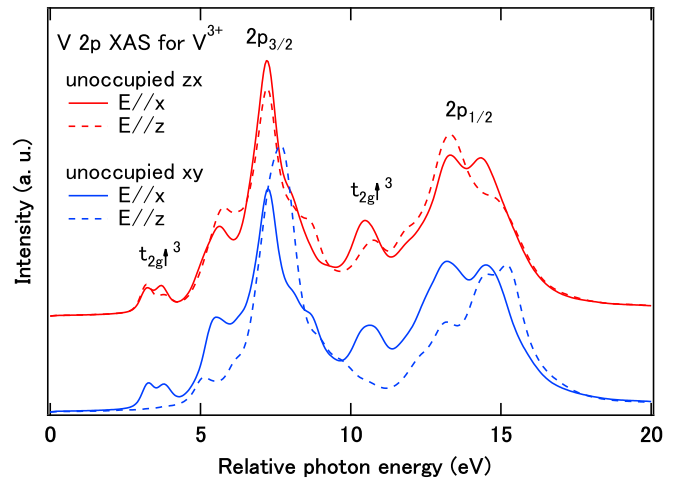


FIG. 5. Polarization dependence of the calculated V $2p$ XAS spectra for V^{3+} with different orbital orders. For the orbital order with V $3d yz$ unoccupied, the polarization dependence of the t_{2g}^3 final state is moderate. On the other hand, the orbital order with V $3d xy$ unoccupied is expected to have strong polarization dependence.

In the present case of V_2OPO_4 , the intensity of the near-edge regions is enhanced when the polarization vector is roughly along the x or y axis. This could indicate that the xy orbital is unoccupied at the V^{3+} site. However, since the xy orbital changes sign by the 90° rotation about the z axis, the relationship between polarization dependence and orbital occupation is less clear than for the a_{1g} orbital. Figure 5 shows the calculated V $2p$ XAS spectra for the polarizations along the x and z axes for the unoccupied zx case and the unoccupied xy case. In the unoccupied zx orbital case, the near-edge regions at 514 and 521 eV are slightly enhanced with the polarization vector along the x axis, which is consistent with the experimental result. As for the unoccupied xy orbital case, the near-edge regions are completely suppressed with the polarization vector along the z axis, inconsistent with the experimental result. The comparison between the experiment and the calculation supports the orbital order with the zx (or yz) orbital unoccupied. The occupied xy orbitals provide a kind of repulsive interaction to the V^{2+} and V^{3+} pairs which is removed by the charge transfer between them. Therefore, the present orbital ordering is consistent with the NTE.

In the V chains running along the $[110]$ or $[1\bar{1}0]$ directions, the $V^{2+}O_6$ and $V^{3+}O_6$ octahedra share their faces. Focusing on the V chains along the $[110]$ directions, the XAS results indicate that the V $3d t_{2g} xy$ and yz (or zx) orbitals are occupied at the V^{3+} site. Here, the x , y , and z axes are close to the $[201]$, $[021]$, and $[001]$ directions of the monoclinic structure, as shown in Fig. 1(a). (The z direction is tilted by about 20° from the $[001]$ direction.) Since the superexchange pathways for the xy , yz , and zx orbitals are all active in the face-sharing V-O-V bond, the V^{3+} and V^{2+} sites should have antiferromagnetic coupling, in agreement with the neutron result [13]. This situation is different from the ferromagnetic coupling between the face-sharing V^{3+} and V^{2+} in $BaV_{10}O_{15}$ and related systems where the a_{1g} orbital is unoccupied at the V^{3+} site [26–28].

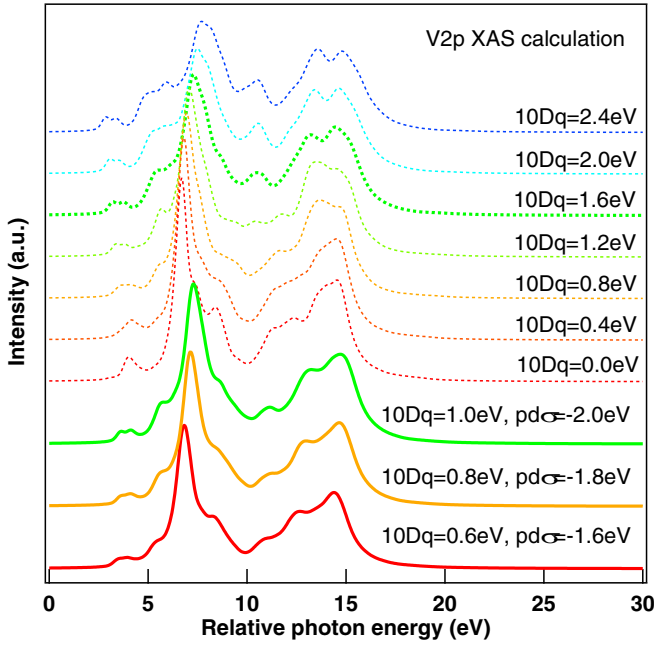


FIG. 6. Effect of the charge transfer process on the V 2p XAS calculation for V^{3+} . The dotted (solid) curves indicate the calculations without (with) the charge transfer process.

It is possible to analyze V 2p XAS considering charge transfer from O 2p to V 3d if charge transfer satellites are observed in the higher-energy region. In the present case, the higher-energy region of the V 2p spectrum is occupied by the O 1s spectrum, and consequently, charge transfer satellites cannot be observed. Here, we theoretically examine the effect of the charge transfer process on the multiplet structure. Without the charge transfer process, the multiplet structure of V 2p XAS for $V^{3+}(d^2)$ strongly depends on the ligand field splitting of $10Dq$ as shown in Fig. 6. Therefore, $10Dq$ is an adjustable parameter in the calculation without the charge transfer process. Since the ligand field splitting is mainly due to the covalency between the transition-metal d orbitals and the ligand orbitals, $10Dq$ can be replaced by parameters such as Δ , U , and $(pd\sigma)$ in the calculation with the charge transfer process. In addition to the covalency effect, there exists an additional $10Dq$ which can be assigned to the effect of nonorthogonality between the transition-metal d orbitals and the ligand orbitals and can be obtained from the transfer and overlap integrals [20]. With $\Delta = 6.0$ eV, $U = 5.0$ eV, $(pd\sigma) = -2.0$ eV, and $10Dq = 1.0$ eV due to nonorthogonality, the multiplet structure roughly resembles that obtained with $10Dq = 1.6$ eV by the calculation neglecting charge transfer. This result supports the analysis neglecting charge transfer in the previous paragraphs.

For face-sharing octahedra in the chains, it is often convenient to use a_{1g} and e_g^π trigonal orbitals. Their forms are given by $(xy - e^{2\pi ni/3}zx - e^{-2\pi ni/3}yz)/\sqrt{3}$, with $n = 0$ for the a_{1g} state and $n = \pm 1$ for two e_g^π orbitals [the a_{1g} orbital points to the (1, 1, -1) direction of the VO_6 octahedron for the case shown in Fig. 1] [2]. One can show that the electron hopping along chains is diagonal for these orbitals [29], which immediately gives the dominant antiferromagnetic coupling

along the chains if the same orbitals are occupied at each site. However, the use of these orbitals is not convenient to treat interchain exchange. Besides that, as mentioned above, in V_2OPO_4 there exists strong distortion of VO_6 octahedra along the local z (or z') directions. Therefore, it is more natural to use the local xy , zx , and yz orbitals that we use in this paper. The xy and yz (or zx) orbitals are given by $(a_{1g} + e_{g+}^\pi + e_{g-}^\pi)/\sqrt{3}$ and $-(a_{1g} + e^{2\pi i/3}e_{g+}^\pi + e^{-2\pi i/3}e_{g-}^\pi)/\sqrt{3}$ [or $-(a_{1g} + e^{-2\pi i/3}e_{g+}^\pi + e^{2\pi i/3}e_{g-}^\pi)/\sqrt{3}$]. Therefore, in the electronic configuration with xy and yz occupied, the a_{1g} , e_{g+}^π , and e_{g-}^π orbitals are equally occupied. Since the a_{1g} , e_{g+}^π , and e_{g-}^π electrons at the V^{2+} site can be transferred to the a_{1g} , e_{g+}^π , and e_{g-}^π orbitals at the V^{3+} site, the superexchange interaction is antiferromagnetic.

In the case of the V chains along the $[1\bar{1}0]$ directions, the z' axis is close to the $[001]$ direction and the polarization vector in the experiment. It can be assumed that the V 3d t_{2g} $x'y'$ and $y'z'$ (or $z'x'$) orbitals are occupied at the V^{3+} site in the $[1\bar{1}0]$ chains. As for the superexchange pathways between the V^{2+} site in the $[110]$ chain and the V^{3+} site in the $[1\bar{1}0]$ chain (the V-O-V bond angle is about 124°), all the t_{2g} electrons of the V^{2+} site can be transferred to the $x'y'$ and $y'z'$ (or $z'x'$) orbitals at the V^{3+} site which is already occupied by electrons. Therefore, the superexchange interaction is expected to be antiferromagnetic, which is also consistent with the neutron result [13].

The superexchange pathways between the two V^{3+} sites in the $[110]$ and $[1\bar{1}0]$ chains are mainly given by those between the yz and $y'z'$ orbitals (also zx and $z'x'$ orbitals) since the V-O-V bond angle is about 132° [see Fig. 1(a)]. If the zx orbital is unoccupied in the chains running along $[110]$ and the $y'z'$ orbital is unoccupied in the chains running along $[1\bar{1}0]$, the two V^{3+} sites along the (001) direction should be ferromagnetic due to the Kugel-Khomskii mechanism [30]. On the other hand, if the zx orbital is unoccupied in the chains running along $[110]$ and the $z'x'$ orbital is unoccupied in the chains running along $[1\bar{1}0]$, the superexchange interaction would be antiferromagnetic. The ferromagnetic V^{3+} - V^{3+} coupling is consistent with the neutron result [13]. Since the charge transfer from the V^{2+} site to the V^{3+} site costs less energy than the other charge transfer processes, the antiferromagnetic couplings between the V^{2+} and V^{3+} sites (both intrachain and interchain) are essential to determine the spin arrangement.

Figures 7(a) and 7(b) show the V 3d and O 2p partial density of states of the ferrimagnetic solution with $U = 5.0$ eV and $J = 0.5$ eV. V 3d electrons of the V^{2+} (V^{3+}) sites mainly contribute to the majority (minority) spin density of states. In Fig. 7(a), the occupied band around -2 eV (minority spin, V^{3+}) is dominated by the XY component. The unoccupied band around 1 eV (minority spin, V^{3+}) is a mixture of ZX and YZ components. Here, the X and Y axes are along the a and b axes, and the Z axis is in the ac plane. The calculated orbital occupation of the V^{3+} site is consistent with the XAS result. It is not obvious why the ZX component is higher than the YZ component in the unoccupied band. We speculate that the global monoclinic structure plays a role rather than the distortion of the VO_6 octahedron. The O 2p partial density of states is consistent with the line shape of O 1s XAS. The lowest-energy unoccupied band around 1 eV corresponds to

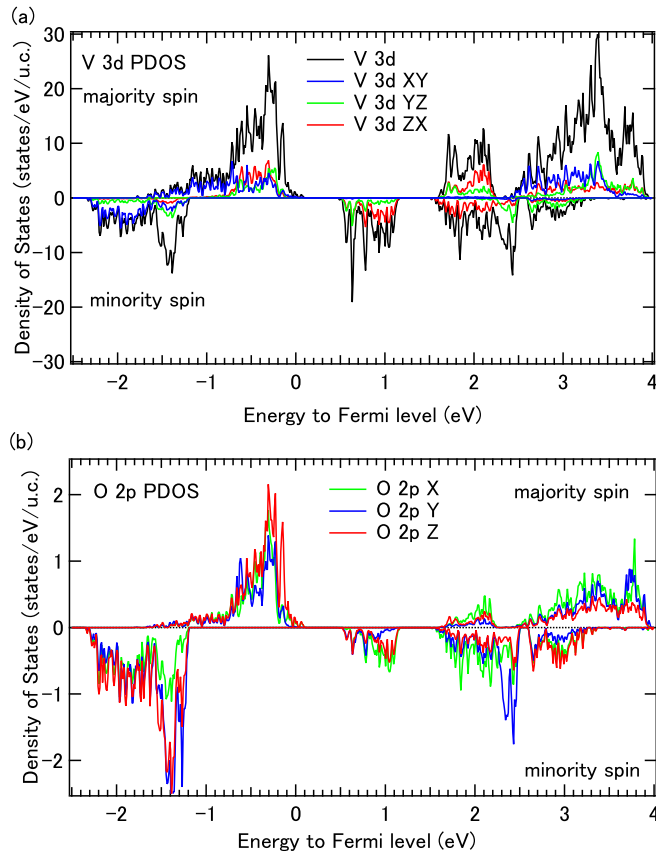


FIG. 7. (a) V 3d partial density of states and (b) O 2p partial density of states obtained by LDA+ U with $U = 5.0$ eV and $J = 0.5$ eV.

the transition to $t_{2g\uparrow}^3$ at V^{3+} . The unoccupied bands ranging from 2 to 4 eV correspond to the transitions to $t_{2g\uparrow}^2 e_{g\uparrow}$, $t_{2g\uparrow}^2 t_{2g\downarrow}$, and $t_{2g\uparrow}^2 e_{g\downarrow}$ at V^{3+} and the transitions from $t_{2g\uparrow}^3$ to $t_{2g\uparrow}^2 e_{g\uparrow}$, $t_{2g\uparrow}^3 t_{2g\downarrow}$, and $t_{2g\uparrow}^3 e_{g\downarrow}$ at V^{2+} . In the lowest-energy unoccupied

band at ~ 1 eV, the amount of O 2p Y is much smaller than those of X and Z components. This is roughly consistent with the polarization dependence of O 1s XAS, although the Z axis is tilted by $\sim 30^\circ$ from the c axis. The consistency between the VO_6 cluster model and the band structure supports the interpretation of the O 1s XAS result [31].

IV. CONCLUSION

In summary, the polarization dependence in near-edge regions of O 1s and V 2p XAS spectra indicates that the xy and zx (or yz) orbitals are occupied in the V^{3+} site. The V 3d orbital order is consistent with the antiferromagnetic coupling between the face-sharing V^{2+} and V^{3+} sites in the chains and the antiferromagnetic coupling between the corner-sharing V^{2+} and V^{3+} sites between the chains. In the future, the relationship between the orbital order and the negative thermal expansion should be investigated by theoretical calculations and experiments at higher temperature.

ACKNOWLEDGMENTS

The authors would like to thank Dr. F. He for the technical support at the REIXS beamline of the Canadian Light Source. All of the measurements reported in this paper were performed at the Canadian Light Source, a national research facility of the University of Saskatchewan, which is supported by the Canada Foundation for Innovation (CFI), the Natural Sciences and Engineering Research Council (NSERC), the National Research Council (NRC), the Canadian Institutes of Health Research (CIHR), the government of Saskatchewan, and the University of Saskatchewan. The work at Waseda was partially supported by CREST-JST (Grant No. JPMJCR15Q2) and KAKENHI from JSPS (Grants No. 19H01853 and No. 19H00659). The work at Edinburgh was supported by EPSRC and ERC. The work of D.I.K. was funded by the Deutsche Forschungsgemeinschaft (DFG, German Research Foundation), Project No. 277146847 - CRC 1238.

- [1] M. Imada, Y. Tokura, and A. Fujimori, *Rev. Mod. Phys.* **70**, 1039 (1998).
- [2] D. I. Khomskii, *Transition Metal Compounds* (Cambridge University Press, Cambridge, 2014).
- [3] J. S. O. Evans, *Dalton Trans.* **3**, 3317 (1999).
- [4] A. W. Sleight, *Curr. Opin. Solid State Mater. Sci.* **3**, 128 (1998).
- [5] K. Takenaka, *Sci. Technol. Adv. Mater.* **13**, 013001 (2012).
- [6] J. Chen, L. Hu, J. Deng, and X. Xing, *Chem. Soc. Rev.* **44**, 3522 (2015).
- [7] S. Ishiwata, M. Azuma, M. Takano, E. Nishibori, M. Takata, M. Sakata, and K. Kato, *J. Mater. Chem.* **12**, 3733 (2002).
- [8] M. Azuma, S. Carlsson, J. Rodgers, M. G. Tucker, M. Tsujimoto, S. Ishiwata, S. Isoda, Y. Shimakawa, M. Takano, and J. P. Attfield, *J. Am. Chem. Soc.* **129**, 14433 (2007).
- [9] M. Mizumaki, N. Ishimatsu, N. Kawamura, M. Azuma, Y. Shimakawa, M. Takano, and T. Uozumi, *Phys. Rev. B* **80**, 233104 (2009).
- [10] S. Ishiwata, M. Azuma, M. Hanawa, Y. Moritomo, Y. Ohishi, K. Kato, M. Takata, E. Nishibori, M. Sakata, I. Terasaki, and M. Takano, *Phys. Rev. B* **72**, 045104 (2005).
- [11] M. Azuma, W.-T. Chen, H. Seki, M. Czapski, S. Olga, K. Oka, M. Mizumaki, T. Watanuki, N. Ishimatsu, N. Kawamura, S. Ishiwata, M. G. Tucker, Y. Shimakawa, and J. P. Attfield, *Nat. Commun.* **2**, 347 (2011).
- [12] K. Oka, M. Mizumaki, C. Sakaguchi, A. Sinclair, C. Ritter, J. P. Attfield, and M. Azuma, *Phys. Rev. B* **88**, 014112 (2013).
- [13] E. Pachoud, J. Cumby, C. T. Lithgow, and J. P. Attfield, *J. Am. Chem. Soc.* **140**, 636 (2018).
- [14] K. Homma and F. Izumi, *J. Appl. Crystallogr.* **44**, 1272 (2011).
- [15] D. G. Hawthorn, F. He, L. Venema, H. Davis, A. J. Achkar, J. Zhang, R. Sutarto, H. Wadati, A. Radi, T. Wilson, G. Wright, K. M. Shen, J. Geck, H. Zhang, V. Novk, and G. A. Sawatzky, *Rev. Sci. Instrum.* **82**, 073104 (2011).

- [16] A. E. Bocquet, T. Mizokawa, K. Morikawa, A. Fujimori, S. R. Barman, K. Maiti, D. D. Sarma, Y. Tokura, and M. Onoda, *Phys. Rev. B* **53**, 1161 (1996).
- [17] T. Mizokawa and A. Fujimori, *Phys. Rev. B* **54**, 5368 (1996).
- [18] F. M. F. de Groot, J. C. Fuggle, B. T. Thole, and G. A. Sawatzky, *Phys. Rev. B* **42**, 5459 (1990).
- [19] K. Okada and A. Kotani, *J. Electron Spectrosc. Relat. Phenom.* **71**, R1 (1995).
- [20] T. Mizokawa, A. Fujimori, T. Arima, Y. Tokura, N. Mōri, and J. Akimitsu, *Phys. Rev. B* **52**, 13865 (1995).
- [21] P. Giannozzi *et al.*, *J. Phys.: Condens. Matter* **21**, 395502 (2009).
- [22] P. Giannozzi *et al.*, *J. Phys.: Condens. Matter* **29**, 465901 (2017).
- [23] H. F. Pen, J. van den Brink, D. I. Khomskii, and G. A. Sawatzky, *Phys. Rev. Lett.* **78**, 1323 (1997).
- [24] J.-H. Park, L. H. Tjeng, A. Tanaka, J. W. Allen, C. T. Chen, P. Metcalf, J. M. Honig, F. M. F. de Groot, and G. A. Sawatzky, *Phys. Rev. B* **61**, 11506 (2000).
- [25] C. F. Chang, T. C. Koethe, Z. Hu, J. Weinen, S. Agrestini, L. Zhao, J. Gegner, H. Ott, G. Panaccione, H. Wu, M. W. Haverkort, H. Roth, A. C. Komarek, F. Offi, G. Monaco, Y.-F. Liao, K.-D. Tsuei, H.-J. Lin, C. T. Chen, A. Tanaka, and L. H. Tjeng, *Phys. Rev. X* **8**, 021004 (2018).
- [26] T. Yoshino, M. Okawa, T. Kajita, S. Dash, R. Shimoyama, K. Takahashi, Y. Takahashi, R. Takayanagi, T. Saitoh, D. Ootsuki, T. Yoshida, E. Ikenaga, N. L. Saini, T. Katsufuji, and T. Mizokawa, *Phys. Rev. B* **95**, 075151 (2017).
- [27] S. Dash, M. Okawa, T. Kajita, T. Yoshino, R. Shimoyama, K. Takahashi, Y. Takahashi, R. Takayanagi, T. Saitoh, D. Ootsuki, T. Yoshida, E. Ikenaga, N. L. Saini, T. Katsufuji, and T. Mizokawa, *Phys. Rev. B* **95**, 195116 (2017).
- [28] S. Dash, M. Okawa, T. Kajita, T. Yoshino, R. Shimoyama, K. Takahashi, Y. Takahashi, R. Takayanagi, T. Saitoh, A. Yasui, E. Ikenaga, N. L. Saini, T. Katsufuji, and T. Mizokawa, *Phys. Rev. B* **99**, 035122 (2019).
- [29] K. I. Kugel, D. I. Khomskii, A. O. Sboychakov, and S. V. Streltsov, *Phys. Rev. B* **91**, 155125 (2015).
- [30] K. I. Kugel and D. I. Khomskii, *JETP Lett.* **15**, 629 (1972) [*Sov. Phys. Usp.* **25**, 231 (1982)].
- [31] S. Lafuerza, G. Subías, J. García, S. Di Matteo, J. Blasco, V. Cuartero, and C. R. Natoli, *J. Phys.: Condens. Matter* **23**, 325601 (2011).